Materials Science-Poland, 32(2), 2014, pp. 193-197
http://www.materialsscience.pwr.wroc.pl/
DOI: 10.2478/s13536-013-0171-z

VERSITA

Influence of different materials on the microstructure and optical band gap of α-Fe_2O_3 nanoparticles

P. MALLICK*

Department of Physics, North Orissa University, Takatpur, Baripada 757003, India

Composites of hematite (α-Fe_2O_3) nanoparticles with different materials (NiO, TiO_2, MnO_2 and Bi_2O_3) were synthesized. Effects of different materials on the microstructure and optical band gap of α-Fe_2O_3 nanoparticles were studied. Crystallite size and strain analysis indicated that the pure α-Fe_2O_3 nanoparticles were influenced by the presence of different materials in the composite sample. Crystallite size and strain estimated for all the samples followed opposite trends. However, the value of direct band gap decreased from ~2.67 eV for the pure α-Fe_2O_3 nanoparticles to ~2.5 eV for α-Fe_2O_3 composites with different materials. The value of indirect band gap, on the other hand, increased for all composite samples except for α-Fe_2O_3/Bi_2O_3.

Keywords: *iron oxide; composite; microstructure; UV-Vis spectroscopy*

1. Introduction

In recent years, research on nanocomposite materials composed of nanometer-sized magnetic particles has been a subject of intense interest since the composites exhibit unique electronic, magnetic and optical properties [1]. Among various magnetic systems, iron oxides, especially hematite (α-Fe_2O_3) has attracted considerable attention as it is widespread in nature, nontoxic and an important industrial product [2–4]. It has been observed that the properties of α-Fe_2O_3 improve when it is used as a composite with other materials. α-Fe_2O_3 composites with different materials have been considered as potential candidates for pseudocapacitors, photocatalysis, high-performance anode material for lithium ion batteries, electromagnetic wave absorption materials etc. Sarkar et al. [5] have reported that α-Fe_2O_3/MnO_2 nanoheterostructures exhibit excellent specific capacitance, high energy density, high power density, and long-term cyclic stability as compared with the bare α-Fe_2O_3 nanowire electrodes. Their studies indicated that the α-Fe_2O_3/MnO_2 nanoheterostructure architecture is very promising for the next-generation high-performance pseudocapacitors. Tang et al. [6] have reported that α-Fe_2O_3/TiO_2 composite hollow spheres show magnetic characteristics at room temperature and good photocatalytic activity under visible-light irradiation compared to the single-component α-Fe_2O_3 particles. Enhanced photocatalytic activity has been observed for α-Fe_2O_3/graphene oxide composite [7, 8]. McDonald et al. [9] have shown that Fe_2O_3/$ZnFe_2O_4$ composite electrode shows a significantly enhanced photocurrent response for use in solar water oxidation as compared to the bare Fe_2O_3 electrode. Zhu et al. [10] have reported that reduced graphene oxide (RG-O)/Fe_2O_3 composite shows improvement of electrochemical performance as compared to pure RG-O and nanoparticle Fe_2O_3. Their study indicated that the nanostructured RG-O/Fe_2O_3 composite can be used as a high-performance anode material for lithium ion batteries. RG-O/Fe_2O_3 composite has also been shown to exhibit excellent microwave absorbability, appropriate to use it as a high performance electromagnetic wave absorption material [11]. Xiao et al. [12] have synthesized Fe_2O_3/graphene composites with different contents of graphene. These authors reported that the composite with graphene mass content of 30 % exhibits excellent cyclability and rate capability in-

*E-mail: pravanjan_phy@yahoo.co.in

dicating the good potential of the composite as an anode material for lithium ion batteries. Cheng et al. [13] have reported that α-Fe_2O_3/C nanocomposite exhibits excellent cycling performance and rate capability as compared to bare α-Fe_2O_3 indicating the composite material as an anode material for lithium-ion batteries.

In the present paper, we study the evolution of microstructure and optical band gap of α-Fe_2O_3 nanoparticle in the presence of different materials (NiO, TiO_2, MnO_2 and Bi_2O_3) in the composite.

2. Experimental

For the preparation of composite samples, α-Fe_2O_3 and NiO nanoparticles were synthesized by chemical route following the procedure adopted in [14]. Commercially available powders of TiO_2, MnO_2 and Bi_2O_3 (all from MERCK, India) were used for making the nanocomposites. A mixture was prepared by taking α-Fe_2O_3 nanoparticles and other materials in the ratio of 0.9:0.1 separately. Then the mixture was grounded thoroughly and pressed to pellets. These pellets were annealed at 500 °C for 1 hour in order to get the required nanocomposite sample.

The structural and microstructural characterizations of composite samples were done by using X-ray diffractometer (Bruker, Model: D8 Advance) with CuKα radiation. UV-Vis characterizations of the samples were performed using diffuse reflectance spectroscopy with a double beam UV-Vis spectrophotometer (Simadzu, UV-2450) equipped with an integrating sphere assembly.

3. Results and discussion

Fig. 1 shows the XRD patterns of α-Fe_2O_3 nanoparticle composites with NiO, TiO_2, MnO_2 and Bi_2O_3. The peaks appearing in the XRD pattern are indexed to the hexagonal structure (space group: $R\bar{3}c$) of α-Fe_2O_3 and they are consistent with the JCPDS No: 33-0664. Inclusion of other materials to the host may influence the microstructure like crystallite size, strain, texture etc. In a recent study, we have shown that the crystallite size and strain of NiO nanoparticles was influenced significantly by making a nanocomposite with CuO [15]. It is noticed from the XRD pattern that the additions of different materials influence the ratio of integrated intensities of (104) to (110) peaks (I_{104}/I_{110}) of the α-Fe_2O_3 nanoparticles. Fig. 2 shows the evolution of I_{104}/I_{110} of α-Fe_2O_3 nanoparticles composites with different materials. This ratio is higher than unity for all the composite samples which corresponds well to the standard XRD pattern of hematite [16]. The ratio of I_{104}/I_{110} in all composite samples except for α-Fe_2O_3/Bi_2O_3 is higher than in the pure α-Fe_2O_3 nanoparticles. Higher I_{104}/I_{110} ratio for the composites than for pure α-Fe_2O_3 nanoparticles indicates the favourable growth direction of the nanoparticles along [104] in the composite [17]. Since the integrated intensities of (104) to (110) peaks of α-Fe_2O_3 nanoparticles were influenced significantly by the additions of different materials, we therefore estimated the average crystallite size (D) and the strain (ε) of the α-Fe_2O_3 nanoparticle composites with other materials from the full width at half maximum (FWHM) of the first two major XRD peaks i.e. (104) to (110) peaks using the following equations [18]:

$$D = \frac{0.94\lambda}{\beta \cos\theta} \tag{1}$$

and

$$\varepsilon = \frac{\beta \cos\theta}{4} \tag{2}$$

where β is the FWHM, θ is the Bragg angle and λ is the wavelength of Cu Kα radiation. The variation of crystallite size and strain for α-Fe_2O_3 nanoparticle composites with different materials are given in Table 1. Crystallite size and strain for all the samples estimated either along [104] or [110] follow an opposite trend. Similar behaviour has been reported for pure α-Fe_2O_3 nanoparticles annealed at different temperatures [14]. Despite the lack of full understanding it can be said at this point that the microstructure of parent α-Fe_2O_3 nanoparticles is influenced by the additions of different materials.

Optical band gaps of α-Fe_2O_3 nanoparticle composites with different materials were estimated by using UV-Vis absorption spectroscopy. Fig. 3

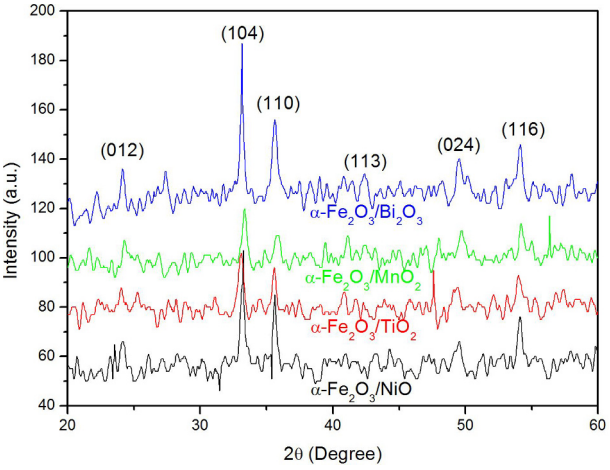

Fig. 1. XRD pattern of α-Fe_2O_3 nanoparticle composites with NiO, TiO_2, MnO_2 and Bi_2O_3.

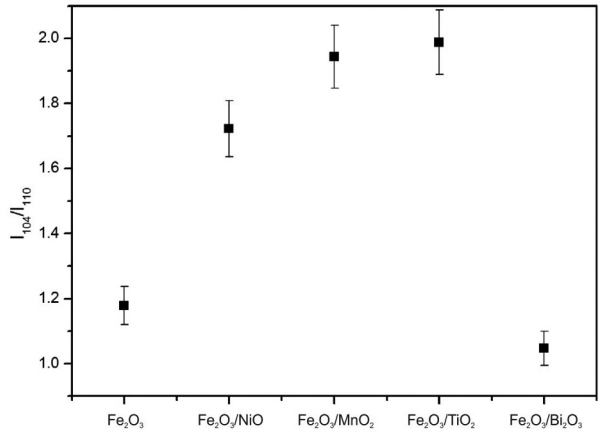

Fig. 2. Variation of I_{104}/I_{110} of α-Fe_2O_3 nanoparticle composites with different materials.

Table 1. Variation of crystallite size and strain of α-Fe_2O_3 nanoparticle composites with different materials.

Sample	Crystallite Size (nm)		Strain (%)	
	along (104)	along (110)	along (104)	along (110)
Fe_2O_3	34.18	33.24	6.1	6.24
Fe_2O_3/NiO	29.27	36.32	7.1	5.7
Fe_2O_3/MnO_2	38.32	33.35	5.4	6.2
Fe_2O_3/TiO_2	31.02	45.02	6.7	4.6
Fe_2O_3/Bi_2O_3	42.89	25.86	5.0	8.0

shows the variation of absorption coefficient, α of α-Fe_2O_3 nanoparticle composites as a function of photon energy. The absorption coefficient for all samples decreased with decreasing energy due to nanocrystalline nature of the material [19]. The optical band gap was extracted from the absorption coefficient according to the following relation [20]:

$$\alpha = \frac{B(h\nu - E_g)^n}{h\nu} \tag{3}$$

where $h\nu$ is the incident photon energy, α is the absorption coefficient, B is a material dependent constant and E_g is the optical band gap. The value of E_g can be determined by extrapolating the linear portion of the $(\alpha h\nu)^{1/n}$ vs. $h\nu$ plot to $\alpha = 0$. In our earlier work, we stated that α-Fe_2O_3 nanoparticles exhibit both direct and indirect band gap [14]. In the present case, we have investigated the occurrence of both direct and indirect transitions by plotting $(\alpha h\nu)^{\frac{1}{n}}$ vs. $h\nu$ with n = 2 (Fig. 4) and $\frac{1}{2}$ (Fig. 5), respectively for all composite samples. The value of direct band gap nanoparticle decreased from ∼2.67 eV for the pure α-Fe_2O_3 [14] to ∼2.5 eV for the α-Fe_2O_3 nanoparticle composites with different materials like NiO, TiO_2, MnO_2 and Bi_2O_3 (Table 2). However, the value of indirect band gap increased for all composite samples except for α-Fe_2O_3/Bi_2O_3. Comparing the crystallite size along [110] (Table 1) with the indirect band gap (Table 2) of a corresponding composite sample, we noticed that the crystallite size along [110] and indirect band gap follow the same trend in the composite sample.

Table 2. Variation of direct and indirect band gap of α-Fe_2O_3 nanoparticle composites with different materials.

Sample	E_g (direct) (eV)	E_g (indirect) (eV)
Fe_2O_3	2.67	1.6
Fe_2O_3/NiO	2.55	1.82
Fe_2O_3/MnO_2	2.53	1.68
Fe_2O_3/TiO_2	2.53	1.91
Fe_2O_3/Bi_2O_3	2.51	1.56

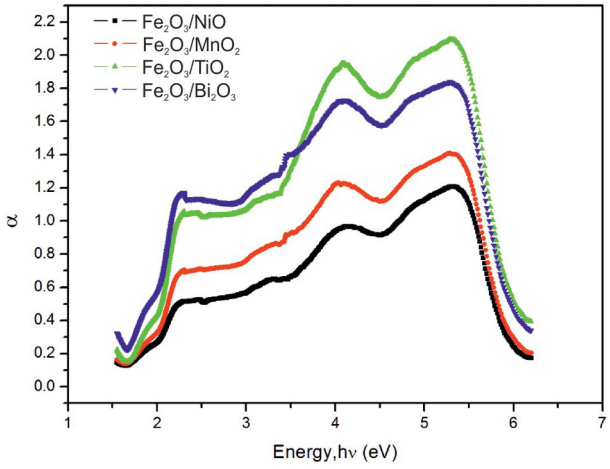

Fig. 3. Variation of absorption coefficient, α vs. photon energy, $h\nu$ for α-Fe_2O_3 nanoparticle composites with NiO, TiO_2, MnO_2 and Bi_2O_3.

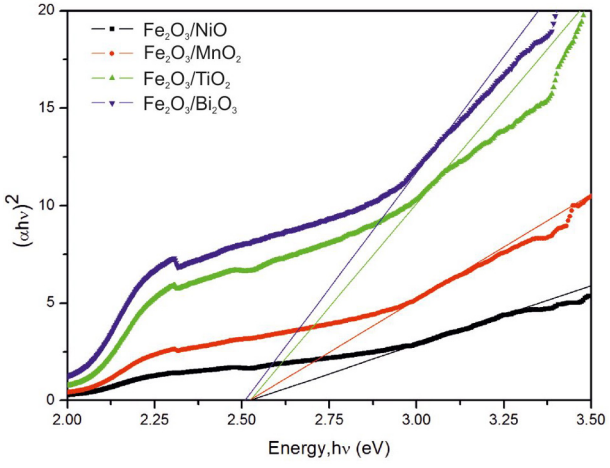

Fig. 4. Variation of $(\alpha h\nu)^2$ vs. photon energy, $h\nu$ for α-Fe_2O_3 nanoparticle composites with NiO, TiO_2, MnO_2 and Bi_2O_3.

4. Conclusions

Hematite (α-Fe_2O_3) nanoparticle composites with different materials (NiO, TiO_2, MnO_2 and Bi_2O_3) were synthesized. Effects of different materials on the microstructure and optical band gap of α-Fe_2O_3 nanoparticles were studied. The presence of different materials in the composite sample influenced the crystallite size and strain of the pure α-Fe_2O_3 nanoparticles significantly. The value of direct band gap decreased from ~2.67 for pure α-Fe_2O_3 nanoparticle to ~2.5 eV for α-Fe_2O_3 composites with different materials. The value of indirect band gap, on the other hand, increased for all composite samples except for α-Fe_2O_3/Bi_2O_3.

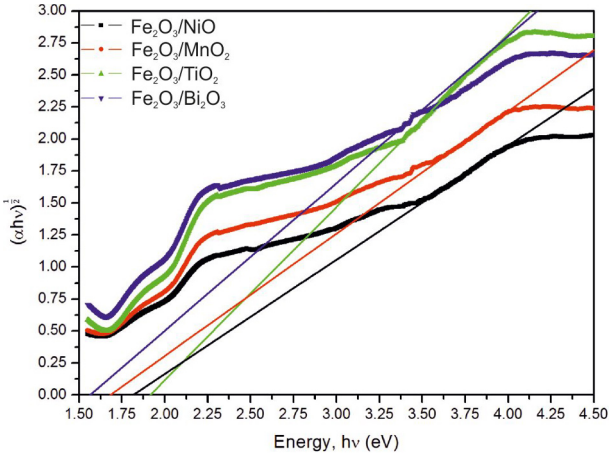

Fig. 5. Variation of $(\alpha h\nu)^{\frac{1}{2}}$ vs. photon energy, $h\nu$ for α-Fe_2O_3 nanoparticle composites with NiO, TiO_2, MnO_2 and Bi_2O_3.

Acknowledgements

The author thanks to Prof. N.C. Mishra, Utkal University, Bhubaneswar for his encouragement and also for providing laboratory facility to carry out this work. DST, Govt. of India is acknowledged for proving XRD facility at Utkal University, Bhubaneswar under FIST programme.

References

[1] BENTIVEGNA F., FERRE J., NYVLT M., JAMET J.P., IMHOFF D., CANVA M., BRUN A., VEILLET P., VISNOVSKY S., CHAPUT F., BOILOT J.P., *J. Appl. Phys.*, 83 (1998), 7776.

[2] VAYSSIERES L., BEERMANN N., LINDQUIST S.-E., HAGFELDT A., *Chem. Mater.*, 13 (2001), 233.

[3] HASSAN M.F., RAHMAN M.M., GUO Z.P., CHEN Z.X., LIU H.K., *Electrochim. Acta*, 55 (2010), 5006.

[4] CHENG F., HUANG K., LIU S., LIU J., DENG R., *Electrochim. Acta*, 56 (2011), 5593.

[5] SARKAR D., KHAN G.G., SINGH A.K., MANDAL K., *J. Phys. Chem. C*, 117 (30) (2013), 15523.

[6] TANG H., ZHANG D., TANG G., JI X., LI W., LI C., YANG X., *Ceram. Int.*, 39 (8) (2013), 8633.

[7] PRADHAN G.K., PADHI D.K., PARIDA K.M., *ACS Appl. Mater. Interfaces*, 5 (18) (2013), 9101.

[8] LI H., ZHAO Q., LI X., ZHU Z., TADE M., LIU S., *J. Nanopart. Res.*, 15 (2013), 1670.

[9] MCDONALD K.J., CHOI K.-S., *Chem. Mater.*, 23 (21) (2011), 4863.

[10] ZHU X., ZHU Y., MURALI S., STOLLER M.D., RUOFF R.S, *ACS Nano*, 5 (4) (2011), 3333.

[11] ZHANG H., XIE A., WANG C., WANG H., SHEN Y., TIAN X., *J. Mater. Chem. A*, 1 (2013), 8547.
[12] XIAO W., WANG Z., GUO H., LI X., WANG J., HUANG S., GAN L., *Appl. Surf. Sci.*, 266 (2013), 148.
[13] CHENG F., HUANG K., LIU S., LIU J., DENG R., *Electrochim. Acta*, 56 (2011), 5593.
[14] MALLICK P., DASH B.N., *J. Nanosci. Nanotechnol.*, 3 (2013), 130.
[15] MALLICK P., SAHOO C.S., *J. Nanosci. Nanotechnol.*, 3 (2013), 52.
[16] FOUDA M.F.R., ELKHOLY M.B., MOSTAFA S.A., HUSSIEN A.I., WAHBA M.A., EL-SHAHAT M.F., *Adv. Mat. Lett.*, 4 (5) (2013), 347.
[17] ZHONG M., LIUY Z., ZHONG X., YU H., ZENG D., *J. Mater. Sci. Technol.*, 27 (11) (2011), 985.
[18] GORDILLO G., FLOREZ J.M., HERNANDEZ L.C., *Sol. Energ. Mat. Sol. C.*, 37 (1995), 273.
[19] CHENG K., HE Y.P., MIAO Y.M., ZOU B.S., WANG Y.G., WANG T.H., ZHANG X.T., DU Z.L., *J. Phys. Chem. B*, 110 (2006), 7259.
[20] MOTT N.F., DAVIS E.A., *Electronic Processes in Non-Crystalline Materials*, Clarendon-Press, Oxford, 1971.

Received 2013-12-17
Accepted 2014-02-05